structures observed by TEM in the amorphous BN obtained by our synthesis.

Although these apparent sites of fiber growth have been identified, little is yet known about the exact mechanism by which the tube growth occurs or the driving forces involved. Although it is difficult to propose a mechanism for the formation of the tubes from the amorphous material, it would appear that their consistently parallel orientation is a result of conditions existing during their growth.

To our knowledge, hollow BN fibers of this type have not been reported previously. Although small, poorly crystalline BN fibrils of approximate dimensions 1 μm by 5 μm have been obtained by high-pressure pyrolysis of borazine (*12*), no indication was given of their internal structure.

REFERENCES AND NOTES

1. J. Thomas, N. W. Weston, T. E. O'Connor, *J. Am. Chem. Soc.* **84**, 4619 (1963).
2. R. T. Paine and C. K. Narula, *Chem. Rev.* **90**, 73 (1990).
3. In a typical trial in an evacuated heavy-walled glass bomb, *B*-trichloroborazine (1.72 g, 9.36 mmol) and metallic cesium (0.99 g, 7.45 mmol) reacted to produce BN [0.25 g, 55% yield based on consumed $(BClNH)_3$]. The reactants must be loaded into the bomb in an inert atmosphere dry-box because of the extremely high reactivity of cesium. Liberated HCl and H_2 were pumped away, unreacted *B*-trichloroborazine was removed by vacuum sublimation, and the CsCl by-product was removed by washing with water.
4. Diffuse reflectance infrared spectra (IR) were recorded with a Mattson Polaris Fourier transform IR spectrometer equipped with diffuse reflectance apparatus. X-ray powder patterns were obtained on a Rigaku Geigerflex powder diffractometer with a Cu target. Scanning electron microscopy was carried out with a JEOL 840 SEM. Energy-dispersive x-ray analysis was performed with a JEOL 820 SEM and a Link Analytical Oxford Instruments eXL EDS. Transmission electron microscopy was generally performed on a JEOL 200CX TEM, with high-resolution TEM and EELS being done on a JEOL 2010 TEM and a Gatan 666 PEELS, respectively.
5. P. J. Fazen, J. S. Beck, A. T. Lynch, E. E. Remsen, L. G. Sneddon, *Chem. Mater.* **2**, 96 (1990).
6. F. A. Miller and C. H. Wilkins, *Anal. Chem.* **24**, 1253 (1952); E. G. Brame, Jr., J. L. Margrave, V. W. Meloche, *J. Inorg. Nucl. Chem.* **5**, 48 (1957).
7. Y. Matsui, Y. Sekikawa, T. Ishii, S. Isakosawa, K. Shii, *J. Mater. Sci.* **16**, 1114 (1981).
8. S. Iijima, *Nature* **354**, 56 (1991).
9. D. Ugarte, *ibid.* **359**, 707 (1992).
10. See, for example, D. J. Smith, M. R. McCartney, E. Tracz, T. Borowiecki, *Ultramicroscopy* **34**, 54 (1990); I. Alstrup, *J. Catal.* **109**, 241 (1988), and references therein.
11. It should also be noted that a similar ED pattern was obtained from the material prior to the 1100°C heating step, which was shown to be amorphous to x-rays. This result might be explained by the presence of some more ordered areas within the essentially amorphous sample. The coexistence of crystalline and amorphous domains in fabricated BN fibers has been shown previously by ED; see D. A. Lindquist, J. F. Janik, A. K. Datye, R. T. Paine, J. B. Rothman, *Chem. Mater.* **4**, 17 (1992).
12. S.-I. Hirano, T. Yogo, S. Asada, S. Naka, *J. Am. Ceram. Soc.* **72**, 66 (1989).

13. We thank the Army Research Office for support of this work through grant DAAL03-92-G-0199. Energy-dispersive x-ray analyses were obtained by J. Mitchell of the Department of Geological Sciences of Ohio State University.

1 February 1993; accepted 25 March 1993

Banded Surface Flow Maintained by Convection in a Model of the Rapidly Rotating Giant Planets

Zi-Ping Sun, Gerald Schubert,* Gary A. Glatzmaier

In three-dimensional numerical simulations of a rapidly rotating Boussinesq fluid shell, thermally driven convection in the form of columns parallel to the rotation axis generates an alternately directed mean zonal flow with a cylindrical structure. The mean structure at the outer spherical surface consists of a broad eastward flow at the equator and alternating bands of westward and eastward flows at higher latitudes in both hemispheres. The banded structure persists even though the underlying convective motions are time-dependent. These results, although still far from the actual motions seen on Jupiter and Saturn, provide support for theoretical suggestions that thermal convection can account for the remarkable banded flow structures on these planets.

The differential rotation on the surface of the sun is characterized by one broad eastward jet in the equatorial region with high-latitude subrotation relative to the basic rotation rate (*1, 2*). The surface differential rotation patterns on Jupiter and Saturn consist of a strong eastward jet in the equatorial region with weaker alternating westward and eastward jets extending up to 80° latitude in each hemisphere (*3, 4*). The latitudinal structure and amplitude of Jupiter's banded zonal surface flow remained essentially constant in time during the 4 months between the Voyager 1 and Voyager 2 encounters (*3*).

Busse (*5*) introduced an analytical model showing how thermal convection in a deep rapidly rotating spherical shell might maintain a mean zonal flow and applied the model to the sun, Jupiter, and Saturn (*6*). Busse hypothesized cylindrically layered convective columnar structures aligned parallel to the axis of planetary rotation, with each convective column drifting longitudinally with constant angular velocity as part of an ordered multilayered configuration. There have been many attempts to simulate numerically the highly nonlinear convective motions and differential rotation in these internally heated rotating fluid bodies (*7–11*). A differential rotation in the form of an equatorial acceleration similar to that observed on the solar surface has been simulated with three-dimensional models of deep convection in a rotating spherical shell (*7–10*). Large eddy diffusivities were used to mimic the subgrid-scale transport of heat and momentum. In these computations, the convergence of angular momentum flux in the equatorial region maintains the differential rotation, but the angular velocity in the interior is predicted to increase with cylindrical radius and to be constant on coaxial cylinders, in contrast to the pattern inferred from helioseismology where angular velocity is constant on spheres (*4*).

One cannot invoke such large eddy diffusivities for Jupiter or Saturn because the small luminosities (internally generated heat fluxes) of these giant planets produce buoyancy forces too weak to overcome the stabilization of large viscous and thermal diffusivities. Small eddy diffusivities lead to small spatial velocity scales, which are ultimately responsible for the banded differential rotation seen on the giant planets. It is the combination of small luminosity and rapid rotation that makes numerical simulation of the giant planets so challenging. A banded differential rotation pattern similar to what is observed has been simulated by modeling Jupiter's shallow gaseous weather layer with a one-level quasi-barotropic model and a two-level quasi-geostrophic model (*11*). However, these shallow layer models neglect the internal heat flux, which is known to be important for the dynamics (*3*), ignore any influence from the vast convecting liquid interior below, and assume that the differential rotation is maintained only by two-dimensional turbulence and baroclinic instabilities in the surface layer.

According to Busse (*6*), a multilayered structure of columnar convection along cylindrical surfaces parallel to the axis of rotation will generate banded east-west surface flow by the convergence of angular

Z.-P. Sun, Department of Atmospheric Sciences, University of California, Los Angeles, CA 90024.
G. Schubert, Department of Earth and Space Sciences and the Institute of Geophysics and Planetary Physics, University of California, Los Angeles, CA 90024.
G. A. Glatzmaier, Earth and Environmental Sciences Division and the Institute of Geophysics and Planetary Physics, Los Alamos National Laboratory, Los Alamos, NM 87545.

*To whom correspondence should be addressed.

momentum flux. Such a multilayered convection pattern in radius is expected to occur at high Taylor number *Ta* (*12*) and Rayleigh number *R* (*13*); in these circumstances, Coriolis and buoyancy forces overwhelm viscous forces and produce north-south convective columns with cross-sectional diameters that are small relative to the depth of the convecting layer. A large *Ta* alone is not sufficient to generate banded differential surface rotation (9).

We have carried out numerical simulations of thermal convection in a rapidly rotating spherical shell of Boussinesq fluid (a fluid of constant density except for thermally induced density variations that generate buoyancy forces) with the purpose of producing a multilayered convection structure in cylindrical radius and an associated banded differential surface rotation. The nonlinear numerical simulations were performed with a three-dimensional time-dependent spectral-transform code (8). The fluid variables were written as sums of reference state and perturbation quantities. The reference state was hydrostatic, spherically symmetric (flattening due to basic state rotation was neglected), and independent of time. The perturbation variables are three-dimensional and time-dependent; they were expanded in spherical harmonics to represent horizontal structure and in Chebyshev polynomials to represent radial structure (*14*).

The inner and outer boundaries of the shell were isothermal, stress free, and impermeable. The dimensionless physical parameters were $Ta = 10^9$, $R = 50R_c$ (R_c is the critical Rayleigh number for onset of convection), and $Pr = 1$ (Pr is the Prandtl number, the ratio of viscous to thermal diffusivity). The values of *Ta* and *R* are not characteristic of Jupiter, for which the values are much larger, but instead are the largest values of these parameters for which numerical solutions were practical. The value $Pr = 1$ may be characteristic of eddy diffusion in Jupiter. The ratio of the inner to outer radius of the deep shell was 0.35, somewhat larger than the ratio of the radius of the silicate core of either Jupiter or Saturn to the respective planetary radius. The spherical shell was heated from below and cooled from above. The numerical solution was calculated with 432 Fourier longitudinal levels, 216 Legendre colatitudinal levels, and 49 Chebyshev radial levels, for a total of nearly 5 million mesh points. Net drops of at least 3.5 orders of magnitude in the kinetic and thermal variances as functions of degree *l* and order *m* of the spherical harmonics and the degree of the Chebyshev polynomials were obtained. The numerical time step was limited by the Courant condition because of the fluid velocity in the numerical grid.

A snapshot of the convective structure after 10,000 time steps, starting from ran-

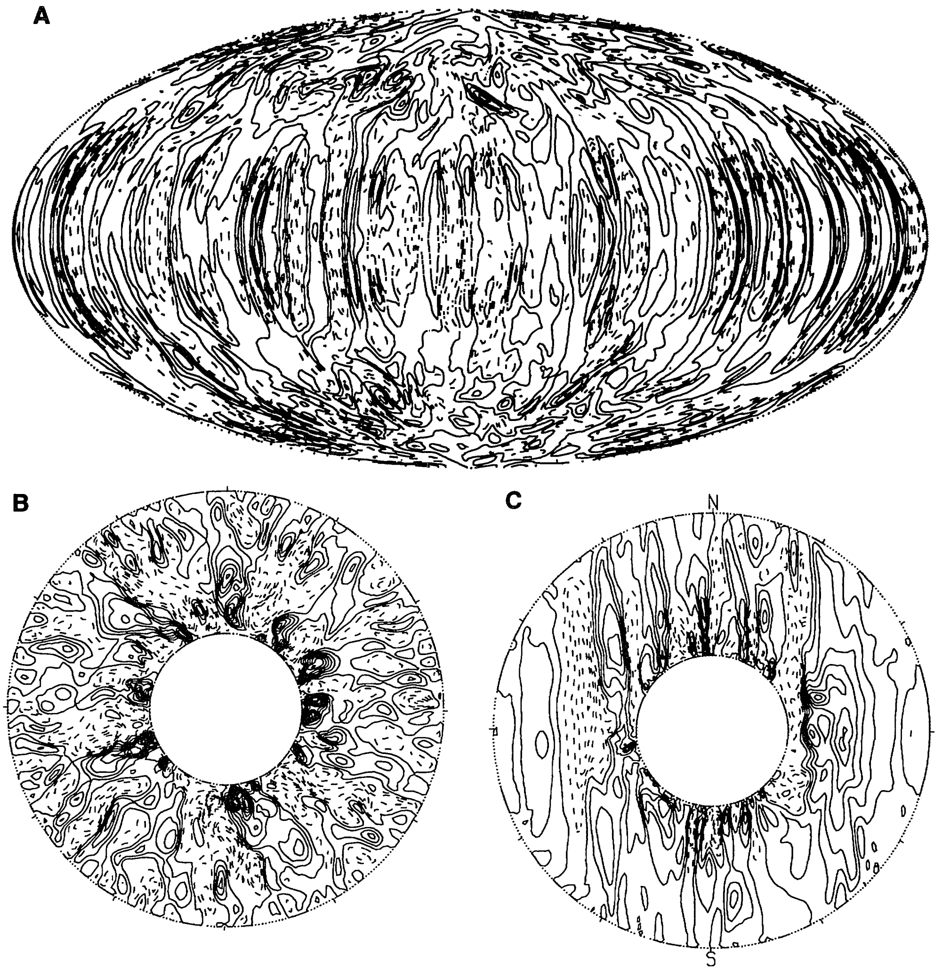

Fig. 1. Contour plots of radial velocity. Solid contours represent outward radial velocities and dashed contours represent inward motions. The zero contour is solid. (**A**) Contours plotted on a spherical surface at a radius $r/r_{top} = 0.87$ (in a Hammer-Aitoff equal area projection). (**B**) Contours plotted in an equatorial plane; 0° longitude is at the top. The direction of the basic rotation is counterclockwise. (**C**) Contours plotted in a meridional cross section (0° longitude on right, 180° on left).

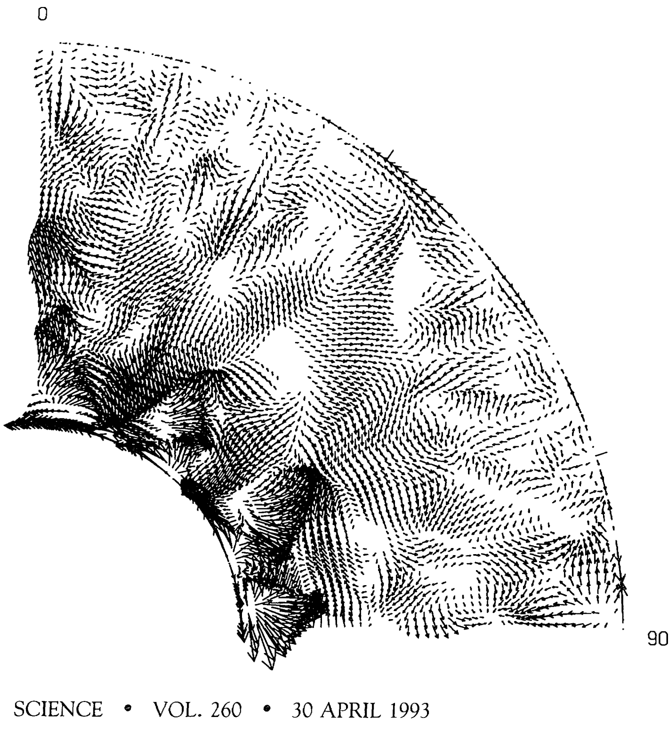

Fig. 2. Velocity vectors in a 90° section of the equatorial plane of the same simulation as in Fig. 1. The arrow lengths are proportional to the velocity amplitudes.

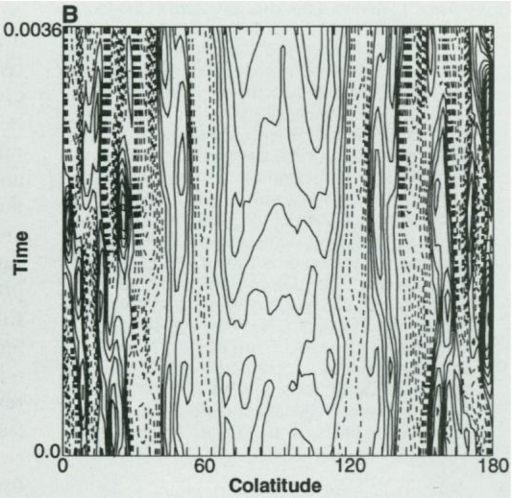

Fig. 3. Contours of longitudinally averaged zonal velocity relative to the basic rotation rate. (**A**) Contours plotted in a meridional plane. Reds represent superrotation (eastward flow) and blues represent subrotation (westward flow). (**B**) Contours in a plot of nondimensional time (vertical coordinate) versus colatitude at a radius of $r/r_{top} = 0.97$. A period of nondimensional time of 3.6×10^{-3} (scaled by d^2/κ) is covered. Solid contours represent superrotation and dashed contours represent subrotation.

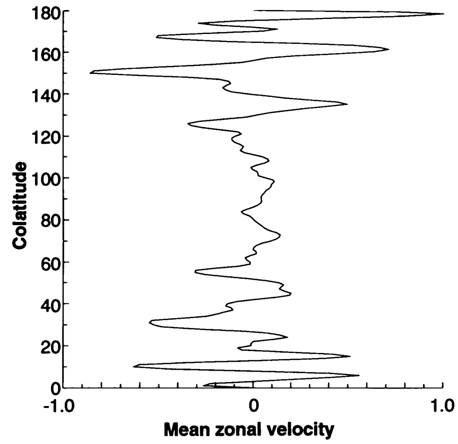

Fig. 4. A snapshot of the longitudinally averaged zonal velocity relative to the basic rotation rate at the surface of the spherical shell. The zonal velocity is normalized by its maximum value.

dom initial conditions, is shown in Figs. 1 and 2. The simulated time is long enough for the decay of initial transients and the establishment of a statistically representative solution. Radial velocity contours on a spherical surface about one-quarter of the shell thickness in from the outer boundary show narrow north-south convective columns at low latitude (Fig. 1A) that represent the structure of convection near the outer boundary in the equatorial region. The dominant longitudinal wave number in this outer convective layer is $m \approx 40$. The convective columns near the inner boundary intersect this surface at high latitude. There are fewer columns around the inner core than around the outer equator. The quasi-layered convective structure in cylindrical radius can also be seen from a snapshot of radial velocity in the equatorial plane (Fig. 1B), and a snapshot of radial velocity in a meridional plane depicts the quasi-layered columnar structure (Fig. 1C). Figure 2 is a snapshot of the velocity vectors in a 90° section of the equatorial plane. The convective patterns are highly time-dependent; seldom do the convective columns complete more than one turnover before changing their patterns. Fluid is continually transported from one convective column to another. Centers of convergence and divergence in this plane are indicative of flow out of the plane in the north-south direction. The instantaneous correlation parallel to the rotation axis of the columnar convection was predicted by the early analytic studies of convection at low R (*1, 5, 6*). However, for the convection described here at high R, the large time-dependence and irregularity of the patterns in planes perpendicular to the rotation axis is unlike the well-organized, multilayered patterns with a uniform drift predicted from the analytic studies.

The generated mean zonal flow (the longitudinally averaged east-west velocity relative to the rotating frame of reference) has a cylindrical structure throughout the deep spherical shell (Fig. 3A). The direction of the mean zonal flow alternates several times in cylindrical radius. The cylindrical zones, outside the tangent cylinder to the inner boundary, intersect the outer spherical surface at roughly the same latitude in each hemisphere. The banded structure persisted in the simulation, although the three-dimensional convection was complicated and time-dependent on small scales (Fig. 3B). When representative values for Jupiter were used to scale the equations, the period of time covered in this plot was about 4 days.

A snapshot of the longitudinally averaged zonal velocity in the outer surface is shown in Fig. 4 in a format similar to that generally used for Jupiter (*3*) and Saturn (*4*). Although the simulated pattern has broad eastward flow in the equatorial region, with alternating east-west jets in each hemisphere, the zonal velocity in the simulation has its greatest amplitude at high latitude rather than in the equatorial region as is seen on Jupiter and Saturn. Also, the amplitude of the axisymmetric zonal velocity is an order of magnitude less than that of the non-axisymmetric velocity. On Jupiter and Saturn, the observed zonal velocity in the equatorial region is about five times larger than the observed root mean square eddy velocities (*3*). Differences between observed and calculated velocities are probably due to the restricted values of Ta, R, and Pr numbers we used because of the limitations of the numerical method and the computing resources (*15*). Nevertheless, the model results show that quasi-layered columnar thermal convection in a deep rapidly rotating spherical shell can maintain a banded zonal differential rotation and thus provide support for the theory that the convergence of angular momentum flux due to columnar convection is responsible for the banded zonal flow patterns observed on the surfaces of Jupiter and Saturn.

REFERENCES AND NOTES

1. P. A. Gilman, *Annu. Rev. Astron. Astrophys.* **12**, 47 (1974).
2. R. Howard and J. Harvey, *Solar Phys.* **12**, 23 (1970); T. M. Brown *et al.*, *Astrophys. J.* **343**, 526 (1989).
3. A. P. Ingersoll *et al.*, *J. Geophys. Res.* **86**, 8733 (1981); R. Beebe, private communication.
4. B. A. Smith *et al.*, *Science* **215**, 504 (1982); R. Beebe, private communication.
5. F. H. Busse, *Astrophys. J.* **159**, 629 (1970).
6. ———, *Icarus* **29**, 255 (1976).
7. P. A. Gilman, *Geophys. Astrophys. Fluid Dyn.* **8**, 93 (1977); *ibid.* **11**, 157 (1978); *ibid.*, p. 181; G. A. Glatzmaier, *Astrophys. J.* **291**, 300 (1985); *Geophys. Astrophys. Fluid Dyn.* **31**, 137 (1985); J. E. Hart, G. A. Glatzmaier, J. Toomre, *J. Fluid Mech.* **173**, 519 (1986); G. A. Glatzmaier and P. Olson, *Geophys. Astrophys. Fluid Dyn.*, in press; Z.-P. Sun, G. Schubert, G. A. Glatzmaier, in preparation.
8. G. A. Glatzmaier, *J. Comp. Physics* **55**, 461 (1984).
9. K.-K. Zhang, *J. Fluid Mech.* **236**, 535 (1992).
10. Z.-P. Sun, G. Schubert, G. A. Glatzmaier, *Geophys. Astrophys. Fluid Dyn.*, in press.

11. G. P. Williams, *J. Atmos. Sci.* 35, 1399 (1978); *ibid.* 36, 932 (1979).
12. The Taylor number Ta is $4\Omega^2 d^4/\nu^2$, where Ω is the basic rotation rate, d is the thickness of the convecting region, and ν is the kinematic viscosity.
13. The Rayleigh number $R = (\alpha\beta\Delta T d^4)/\nu\kappa$ is a measure of the vigor of thermal convection; α is the thermal expansivity, β is $4\pi G\bar{\rho}/3$, G is the gravitational constant, $\bar{\rho}$ is the density of the reference state, and ΔT is the temperature difference across the convecting fluid layer. The definitions of d and ν are in (12), and κ is the thermometric diffusivity.
14. An alias-free spectral transform method was used to compute the nonlinear terms. The time integration treats the nonlinear and Coriolis terms explicitly by an Adams-Bashforth scheme and the linear terms implicitly by a Crank-Nicolson scheme. Numerical stability is maintained by the Courant condition on the time step, and the adequacy of the spatial resolution is checked by calculations at different levels of resolution.
15. Additional calculations have been carried out at values of Ta and R smaller than the values used in the simulation reported here. None of these calculations yielded a banded structure in the longitudinally averaged zonal flow at the surface. The occurrence of banding in the surface zonal flow requires that the north-south convective columns have small diameters compared with the thickness of the convecting shell. This occurs only when both Ta and R are sufficiently large. The spatial resolution of the calculation (in spherical harmonic spectral space all harmonics of degree and order up to 144 were retained) allowed the successful simulation of the small-scale convective structures. The numerical solution reported here was calculated on a Cray YMP8/864 supercomputer at the San Diego Supercomputer Center. It required 256 megabytes of computer memory and 900 hours of CPU time. The solutions at lower values of Ta and R are in (15).
16. This research was supported by grants from the Institute of Geophysics and Planetary Physics at the Los Alamos National Laboratory and the National Aeronautics and Space Administration Ames Research Center.

2 November 1992; accepted 18 March 1993

Water Sources for Subduction Zone Volcanism: New Experimental Constraints

Alison R. Pawley* and John R. Holloway

Despite its acknowledged importance, the role of water in the genesis of subduction zone volcanism is poorly understood. Amphibole dehydration in subducting oceanic crust at a single pressure is assumed to generate the water required for melting, but experimental constraints on the reaction are limited, and little attention has been paid to reactions involving other hydrous minerals. Experiments on an oceanic basalt at pressure-temperature conditions relevant to subducting slabs demonstrate that amphibole dehydration is spread over a depth interval of at least 20 kilometers. Reactions involving other hydrous minerals, including mica, epidote, chloritoid, and lawsonite, also release water over a wide depth interval, and in some subduction zones these phases may transport water to deep levels in the mantle.

Water plays an important role in subduction zones. It is incorporated in basaltic oceanic crust by hydrothermal alteration at mid-ocean ridges, and during subduction it is released in a series of mineral reactions that transform the hydrated basalt to eclogite. Some of this water moves upward and hydrates the mantle wedge overlying the slab. The consistent location of volcanic fronts 100 to 150 km above the slab (*1*, *2*) has been interpreted to be a consequence of dehydration-melting involving amphibole in this hydrated mantle (*2*–*4*). The water may also allow the slab to melt directly if temperatures are high enough and will enhance mineral reactions at otherwise kinetically unfavorable low temperatures. Some water may be retained to great depth in high-pressure hydrous minerals and nominally anhydrous minerals.

A. R. Pawley, Department of Chemistry, Arizona State University, Tempe, AZ 85287.
J. R. Holloway, Department of Chemistry and Department of Geology, Arizona State University, Tempe, AZ 85287.

*To whom correspondence should be addressed.

Despite the obvious importance of hydrous minerals in subduction zones, the pressure-temperature conditions at which dehydration reactions occur in the slab are uncertain. Studies of the wet melting of natural basaltic rocks (*5*, *6*) and peridotitic rocks (*7*, *8*) have shown that amphibole is the most important hydrous phase at high pressures and temperatures in these compositions and indicate that it is stable to higher pressures in peridotitic mantle wedge than in subducted basaltic oceanic crust: ~30 kbar (*7*) versus ~27 kbar (*5*, *6*). However, in these earlier studies amphibole stability was not investigated at temperatures below the wet solidus, which are particularly relevant for subduction zones, and only the final disappearance of the amphibole was documented so that the pressure-temperature interval over which amphibole dehydration occurs is uncertain. We therefore investigated the subsolidus stability of amphibole in a natural oceanic basalt, assumed to be typical of slab basalt.

Although amphibole is certainly the principal hydrous phase in subducting oceanic crust, the need for data on other hydrous minerals (for example, chlorite, epidote, chloritoid, and pumpellyite) has been recognized (*9*). Dehydration of these phases in the slab at a greater depth than amphibole dehydration might produce the fluid involved in the petrogenesis of back-arc basin volcanics (*10*). Therefore, we also investigated the stability of other hydrous phases in basalt at temperatures close to the solidus and near the high-pressure limit of amphibole stability. In addition, to determine whether any hydrous minerals might remain stable within the basaltic part of the slab to much greater depth, we conducted two experiments at ~75 kbar and 1000°C using a basaltic composition and a basanitic composition. The basanitic composition was used to determine whether high concentrations of K and Ti affect the stability of hydrous minerals.

We performed most of the experiments at pressures of 20 to 30 kbar and temperatures of 650 to 725°C using piston-cylinder apparatus (*11*). These conditions were selected to span the expected range of pressure and temperature in subducting slabs after passing through blueschist- and eclogite-facies metamorphic zones (*12*). The starting composition (Table 1) was designed to approximate that of subducted oceanic crust. It consisted of mid-ocean ridge basalt (MORB) with seeds of garnet, omphacitic pyroxene, epidote, sodic amphibole, and phengitic mica to facilitate reaction at low temperatures (*13*). For the two experiments at 75 kbar we used a multianvil apparatus (*14*). The basaltic starting material contained MORB glass, sodic amphibole, lawsonite, quartz, and muscovite. The MORB was replaced by kaersutite amphibole in the basanitic composition (*15*).

Run products were examined under a petrographic microscope and with powder x-ray diffraction. We used Fourier transform infrared spectroscopy (FTIR) to identify hydrous phases and for quantifying modal variations. For standards we used hydroxyl-stretching frequencies obtained from natural samples, as well as published spectra of natural and synthetic samples (*16*). Compositions of some run products were determined by electron microprobe analysis (EMPA).

All run products (Table 1 and Fig. 1), including those produced at 75 kbar and 1000°C, contained garnet, clinopyroxene, and a silica polymorph, either quartz or coesite. Hydrous minerals were produced in all of the experiments at ≤30 kbar. Amphibole was the most abundant phase at 20 kbar, decreased in abundance to 25 kbar, and was absent at 30 kbar; mica and epidote were present in all of these exper-